Desalination and Water Treatment
www.deswater.com

doi: 10.1080/19443994.2016.1195290

57 (2016) 26345–26354
November

Taylor & Francis
Taylor & Francis Group

Modeling the effect of wind in rectangular settling tanks for water supply

Anthoula Gkesouli[a,*], Maria Nitsa[b], Anastasios I. Stamou[a,b], Peter Rutschmann[b], Minh Duc Bui[b]

[a]*Department of Water Resources and Environmental Engineering, School of Civil Engineering, National Technical University of Athens, Heroon Polytechniou 5, 15780 Athens, Greece, Tel. +30 2107722801; Fax: +30 2107722814; email: anthi.gkesouli@gmail.com (A. Gkesouli), Tel. +30 2107722809; Fax: +30 2107722814; email: stamou@central.ntua.gr (A.I. Stamou)*

[b]*Chair of Hydraulic and Water Resources Engineering, Technical University of Munich, Arcisstr. 21, 80333 Munich, Germany, Tel. +30 6942702884; email: ni.maria7@gmail.com (M. Nitsa), Tel. +49 8928923161; Fax: +49 8928923172; email: peter.rutschmann@tum.de (P. Rutschmann), Tel. +49 8928923925; Fax: +49 8928923172; email: bui@tum.de (M.D. Bui)*

Received 22 January 2016; Accepted 22 May 2016

ABSTRACT

A 2-D CFD model is applied to investigate the effect of co-current and counter-current wind velocities of up to 7.5 m/s in the settling tanks of EYDAP Water Treatment Plant of Aharnes, in Greece, and the following conclusions are drawn: (1) without wind, the flow field is characterized by a large recirculation region with significant short-circuiting, while for windy conditions a two-layer flow is observed, in which the surface layer follows the wind direction. The suspended solids' concentration fields strongly depend on the corresponding flow fields. (2) Calculated local removal efficiencies, without wind, near water surface show a satisfactory agreement with measurements. When the sludge removal mechanism is operating, the calculated efficiency without wind is equal to 83.1%; this value is lower than the experimental value (86.0 ± 1.0%) and the predicted value by a 3-D model (85.7%). When co-current wind velocity increases, short-circuiting increases and the efficiency decreases; however, not noticeably (<0.3%). When counter-current wind velocity increases, short-circuiting is reduced and the efficiency increases by up to approximately 1.0%. (3) When the sludge removal mechanism is out of operation, the calculated efficiency without wind decreases to 68.1%, a value that is again lower than the experimental value (70.8 ± 1.0%) and the predicted value by a 3-D model (70.9%); the wind effect is similar to the case of operating sludge removal mechanism, with a somehow larger difference of up to 1.3%.

Keywords: Wind; Settling tank; Water treatment plant; CFD modeling; Suspended solids; Settling efficiency

*Corresponding author.

Presented at CEST2015—14th International Conference on Environmental Science and Technology, Rhodes, Greece, 3–5 September 2015

1. Introduction

Sedimentation is one of the most important treatment processes in conventional Water Treatment Plants (WTPs) and it is performed in settling tanks whose aim is to remove via settling the desired portion of suspended solids (SS) and to achieve the required removal efficiency. The efficiency of settling tanks depends mainly on the characteristics of the flow field, e.g. the distribution of flow velocities and the mixing regime in the tanks, as well as on the characteristics of the SS, e.g. their density, sizes, and settling velocities. In the last three decades, many researchers have developed and applied computational fluid dynamics (CFD) models for the calculation of the flow and SS concentrations' field in the tanks and, subsequently, for determining their removal efficiency. The majority of these applications aim at (1) the design of new tanks or the optimization of the design of existing tanks via the change of various parameters, such as alternative geometrical modifications [1–4], and (2) the study of the effects of various parameters that may affect the efficiency of settling tanks. One of these parameters is the "wind"; generally, it is recognized that the removal efficiency of settling tanks is sensitive to wind effects [3,5] and the wind is among the reasons that decrease the tanks' efficiency [6]. However, in the usual design practice, the wind effect is neglected; subsequently, only a few relevant studies are found in the literature. Sivakumar and Lowe [7] presented a 2-D model, which employed the k–ε turbulence model and the sediment transport equations to investigate the effect of wind on the removal efficiency of a rectangular settling tank. They studied various wind velocities in the co-current and counter-current direction and they drew the following conclusions: (i) the flow field in the tank can be significantly affected by wind action, (ii) with increasing wind velocity, the wind generated re-circulation region in the tank becomes more extended leading to intense mixing and uniform distribution of the SS, (iii) the wind has a detrimental effect on the distribution of SS, and (iv) the removal efficiency decreases with increasing wind velocity with counter-current wind velocity being more significant. Khezri et al. [8] performed an experimental study in a pilot-scale sedimentation tank to determine the effect of wind velocity and direction on the removal efficiency of particles and concluded that (i) the actual efficiency of the tank (61.24%) decreases with co-current wind velocities of 4.5, 5.5, and 7.0 m/s to 50.01, 46.04, and 45.03%, respectively, (ii) for counter-current wind velocity equal to 2.5 m/s the efficiency increases to 65.00% due to an increase in the solids' retention time, and (iii) when the counter-current wind velocity increases to 3.5 and 5.0 m/s, the efficiency decreases to 55.07 and 47.00%, respectively, due to re-suspension of solids. Very recently, Stamou and Gkesouli [9] applied a 3-D CFD model in the rectangular settling tanks of the EYDAP WTP of Aharnes (WTPA) [10] and modeled the effect of the wind (with co-current velocity equal to 15 m/s) by specifying a constant horizontal flow velocity equal to 0.50 m/s on the free surface based on Tsahalis [11]; their results showed that the effect of wind on the flow field was strong with the creation of massive re-circulation areas with intense mixing and high short-circuiting. However, the effect of wind on the removal efficiency of the tanks was not pronounced; the efficiency of the tanks, for an overflow rate equal to OR = 0.85 m/h, which was equal to 72.48% for no-wind conditions, was reduced to 68.07% for windy conditions. In the present work, we apply a 2-D CFD model in the settling tanks of the WTPA to assess the effect of wind on the flow field, SS concentration field, and efficiency of the tanks and to compare the results with these of the 3-D model [9].

2. Equations of the model

The continuity and momentum equations are solved to determine the 2-D flow field in the tank, the free surface is determined with the volume of fluid (VOF) method and the SS concentration field is calculated via the sediment scour model [12].

2.1. Flow field equations

The continuity and momentum equations in a Cartesian coordinate system read as follows [12,13]:

$$V_F \frac{\partial \overline{\rho}}{\partial t} + \frac{\partial}{\partial x^i}\left(\overline{\rho}\overline{u^i}A^i\right) + \frac{\partial}{\partial x^j}\left(\overline{\rho}\overline{u^j}A^j\right) = 0 \quad (1)$$

$$\frac{\partial \overline{u^i}}{\partial t} + \frac{1}{V_F}\left(\overline{u^i}A^i\frac{\partial \overline{u^i}}{\partial x^i} + \overline{u^j}A^j\frac{\partial \overline{u^i}}{\partial x^j}\right) = -\frac{1}{\overline{\rho}}\frac{\partial P}{\partial x^i} + G^i + f^i \quad (2)$$

where V_F is the fractional volume open to the flow, $\overline{\rho}$ is the bulk density of the water–SS mixture, t is the time, P is the pressure, x^i is the Cartesian coordinate in the i-direction, $\overline{u^i}$ is the bulk velocity of the water–SS mixture, A^i is the fractional area open to the flow, G^i is the body acceleration, and f^i is the viscous acceleration in the i-direction.

In the present work, the SS, which have a density (ρ_s) equal to 2,730 kg/m^3, are classified into four (i = 1–4) classes that have different volume concentrations $c_{s,i}$, i.e. volume of class i per volume of water–SS mixture. Using the subscript s,i to denote quantities for each class of SS, we write the equation for the bulk density ($\overline{\rho}$) of the water–SS mixture as follows [14]:

$$\overline{\rho} = \rho_s \sum_{i=1}^{i=4} c_{s,i} + \rho_w \left(1 - \sum_{i=1}^{i=4} c_{s,i}\right) \tag{3}$$

where ρ_w is the density of the water.

The viscous accelerations are calculated by Eq. (4) [12,13]:

$$\overline{\rho} V_F f^i = \tau_{bx^i} - \left[\frac{\partial}{\partial x^i}\left(A^i \tau_{x^i x^i}\right) + \frac{\partial}{\partial x^j}\left(A^j \tau_{x^i x^j}\right)\right] \tag{4}$$

where τ^i_{bx} is the wall shear stress and $\tau_{x^i x^j}$ is the strain rate tensor; the latter are calculated by Eqs. (5) and (6):

$$\tau_{x^i x^i} = -2\mu_{tot}\left(\frac{\partial \overline{u^i}}{\partial x^i}\right) \tag{5}$$

$$\tau_{x^i x^j} = -\mu_{tot}\left(\frac{\partial \overline{u^i}}{\partial x^j} + \frac{\partial \overline{u^j}}{\partial x^i}\right) \tag{6}$$

where $\mu_{tot} = \mu + \mu_T$ is the total dynamic viscosity, μ is the dynamic viscosity, and μ_T is the eddy viscosity. The effect of wind is taken into account via the modification of the shear stress τ on the water surface as follows:

$$\tau = \rho_\alpha c_D W \sqrt{W^2} \tag{7}$$

where ρ_a is the air density, W is the wind velocity at height 10 m above the water surface, and c_D is the drag coefficient, whose values are calculated by Eq. (8) [15]:

$$c_D = 0.565 \times 10^{-3} \quad \text{for } \sqrt{W^2} \le 5 \text{ m/s} \tag{8a}$$

$$c_D = \left(-0.12 + 0.137\sqrt{W^2}\right) \times 10^{-3} \quad \text{for } 5 \text{ m/s} \le \sqrt{W^2} \le 19.22 \text{ m/s} \tag{8b}$$

The eddy viscosity is calculated via the turbulence renormalization group (RNG) model, which is based on the eddy viscosity hypothesis and applies statistical methods for the derivation of the averaged equations for the turbulence kinetic energy (k) and the turbulence dissipation (ε). Moreover, it uses similar equations to the standard k–ε model [16]. However, additional terms exist and the model constants differ since they are derived explicitly and not empirically, as in the standard k–ε model. In general, the RNG model has wider applicability and it is known to describe low intensity turbulence flows and flows having strong shear regions more accurately than the standard k–ε model. The distributions of k and ε are calculated by Eqs. (9) and (10):

$$\frac{\partial(\overline{\rho}k)}{\partial t} + \frac{1}{V_F}\left(\overline{\rho}\overline{u^i}A^i\frac{\partial k}{\partial x^i} + \overline{\rho}\overline{u^j}A^j\frac{\partial k}{\partial x^j}\right) = P_s + G + \text{Diff} - \overline{\rho}\varepsilon \tag{9}$$

$$\frac{\partial(\overline{\rho}\varepsilon)}{\partial t} + \frac{1}{V_F}\left(\overline{\rho}\overline{u^i}A^i\frac{\partial \varepsilon}{\partial x^i} + \overline{\rho}\overline{u^j}A^j\frac{\partial \varepsilon}{\partial x^j}\right) = \frac{1.42\varepsilon}{k}(P_s + 0.2\,G) + \text{DDif} - 1.68\frac{\overline{\rho}\varepsilon^2}{k} \tag{10}$$

where P_s represents the shear production, G is the buoyancy production, and Diff and DDif represent the diffusion; more details for RNG model can be found in [17,18].

2.2. The VOF model

The free surface is handled by the VOF method [19] which determines the volume fraction (F). In this method, the cells of fluid domain are classified as empty, fully filled, or partially filled with fluid while the corresponding volume fraction (F) varies from 0 (empty cells) to 1 (fully filled cells); F is determined by the following transport equation [12]:

$$\frac{\partial F}{\partial t} + \frac{1}{V_F}\left[\frac{\partial}{\partial x^i}\left(FA^i\overline{u^i}\right) + \frac{\partial}{\partial x^j}\left(FA^j\overline{u^j}\right)\right] = 0 \tag{11}$$

The VOF method consists of three components: a scheme to locate the surfaces, a method to track surfaces, and a process to set the appropriate boundary conditions there. In each cell of the computational grid, the value of F is calculated, which is then compared with the values of F in the surrounding cell volumes. The surface slope and the position of the water surface are then determined.

2.3. The sediment scour model

The sediment scour model [14] is used to calculate the SS concentration field in the tank. The concentration of each class of SS is calculated by solving its own transport equation, i.e. SS are transported due to

advection along the water and may settle depending on their settling velocity. For each class, the following transport (advection–diffusion) equation is solved [14]:

$$\frac{\partial C_{s,i}}{\partial t} + u_{s,i}\frac{\partial C_{s,i}}{\partial x^i} = D\frac{\partial^2 C_{s,i}}{\partial x^{i2}} \tag{12}$$

where $C_{s,i}$ is the mass concentration of class i (which is defined as the mass of class i per volume of water–SS mixture), $u_{s,i}$ is the velocity of class i, and D is the diffusivity; $C_{s,i}$ is related to $c_{s,i}$ via Eq. (13):

$$c_{s,i} = \frac{C_{s,i}}{\rho_s} \tag{13}$$

The solution of Eq. (12) requires the calculation of the velocity $u_{s,i}$; assuming that (i) SS do not have strong interactions with each other and (ii) that the velocity difference between the SS and the water–SS mixture is mainly the settling velocity of SS ($u_{\text{set},i}$), the $u_{s,i}$ is calculated by Eq. (14):

$$u_{s,i} = \bar{u} + u_{\text{set},i}c_{s,i} \tag{14}$$

The bulk velocity $\bar{u}$ of the water–SS mixture, which is calculated by Eqs. (1) and (2), is defined as follows:

$$\bar{u} = \sum_{i=1}^{i=4} c_{s,i}u_{s,i} + \left(1 - \sum_{i=1}^{i=4} c_{s,i}\right)u_{\text{w}} \tag{15}$$

where u_{w} is the water velocity.

3. Characteristics of the settling tank

3.1. Geometry of the tank

The top view of the settling tanks of the WTPA is shown in Fig. 1(a); the tanks are rectangular with length equal to 73.2 m, width equal to 14.4 m, and average water depth equal to 3.5 m. Water from flocculation tanks, where aluminum sulfate is used, enters into the settling tanks via four openings that are located near the bottom of the tanks, and exits via a series of V-notch weirs which are installed at three outlet channels; more details can be found in [9,10]. In the present calculations, the geometry of the tank is approximated as 2-D; its longitudinal view is shown in Fig. 1(b). Water enters into the tank via a slot opening equal to 0.15 m and exits via the outlet weir which is located at the end of the effective settling zone, just upstream of the outlet region (x = 63.2 m); see Fig. 1(b). This simplification is made assuming that the volume under the outlet channels is "dead volume", following the approach of Celik et al. [20] and Stamou et al. [21].

3.2. Modes of operation and measurements

Raw water, which is mainly surface water, enters into the WTPA and undergoes firstly coagulation–flocculation process (using aluminum sulfate as flocculant and cationic polyelectrolyte as coagulant aid) and then enters into the settling tanks. In the present work, we considered two modes of operation of the tanks: mode A, when the sludge removal mechanism in the tank was operating, and mode B, when the sludge removal mechanism was out of operation, the sludge was accumulated at the bottom of the tank and was removed periodically. For mode A, extensive laboratory measurements were performed according to the Standards Methods of APHA, AWWA, and WEF [22], as described below, while for mode B the corresponding measurements can be found in Stamou and Gkesouli [9].

(1) Particle size distribution measurements at the inlet of the tank; these were performed using the filtration, based on method 2,540 D [22], in order to classify the SS at the inlet of the tank into 4 classes C1, C2, C3, and C4 which correspond to filter pore sizes equal to 22.5, 11.0, 8.0, and 2.5 μm, respectively, and to determine their percentages (p_{in}) in the mixture, as shown in Table 1. This number of classes was selected after a series of extensive preliminary laboratory measurements starting with 7 filters; obviously, a smaller number of classes, for example, 3, would have resulted in a less detailed description of the suspended particles. In Table 1, the settling velocities of each class using the Stokes' law are also shown, as well as the Hazen number and the removal efficiency of the tank for ideal settling conditions.

Table 1 depicts that the highest percentage (70%) of SS belongs to class C1; these SS have a very high Hazen number and are expected to be completely removed from the tank independently of the flow and, possibly, of the wind conditions; therefore, the removal efficiency of the tank is expected to be higher than 70%. It is also expected that classes C2, C3, and C4 depend on the flow and wind characteristics and that the degree of this dependence increases with decreasing Hazen number.

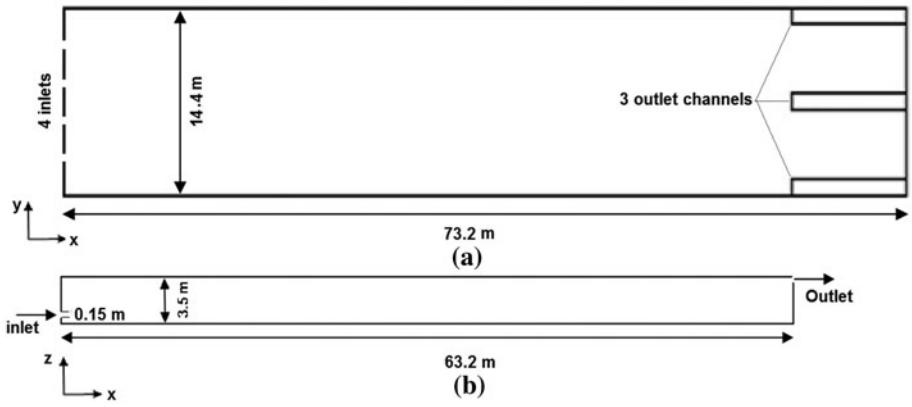

Fig. 1. (a) Top view and (b) longitudinal view of the settling tank.

Table 1
Characteristics of the SS at the inlet of the tank for mode *A*

Class (–)	$d_{r,i}$ (μm)	$d_{c,i}$ (μm)	$u_{\text{set},i}$ (m/h)	p_{in} (%)	C_{in} (mg/L)	Hazen number (–)	R_{ideal} (%)
C1	>22.5	41.0	5.80	70.0	4.9	6.80	100.0
C2	11.0–22.5	17.0	0.96	20.5	1.4	1.12	100.0
C3	8.0–11.0	9.5	0.31	4.0	0.3	0.36	36.0
C4	2.5–8.0	5.0	0.09	5.5	0.4	0.11	11.0
Sum	–	–	–	100	7.0	–	92.5

(2) At the inlet and the outlet of the tank, *in situ* turbidity measurements were performed using a Hach 2100N turbidimeter, as well as SS concentration measurements based on the method 2,540 D [22]; from these measurements, the average value of the removal efficiency of the tank was determined equal to 86.0% and its standard deviation equal to ±1.0%.
(3) Turbidity measurements along the surface of the tank; these were used to determine the local removal efficiencies, after translating turbidity values (NTU) into SS concentrations (SS) via the following linear relationship:

$$\text{SS} = 1.29 \cdot \text{NTU} - 0.35 \tag{16}$$

(4) Visual observations of the lengths of the recirculation region and of the sludge layer (see also Fig. 2), whose average values were determined approximately equal to 20.0 and 45.0 m, respectively, with accuracy equal to ±2.0 m.

Wind velocity and direction were measured with a RNRG 40C anemometer and 200P sensor, respectively; these devices were installed near the inlet of the tank at a height equal to 2.5 m from the water surface. It is noted that the measured removal efficiencies, for both co-current and counter-current wind velocities up to 7.5 m/s, were practically the same with the no-wind conditions.

4. Numerical and calculation details

4.1. Numerical code, calculation domain, boundary conditions, and numerical grid

We employed the CFD code FLOW-3D v.11 [12] that uses the finite control-volume method for the spatial discretization of the domain (see [12] for more details) and we defined boundary conditions at the borders of the calculation domain. At the slot opening, a parallel flow (flow rate equal to 0.26 m^3/s) was imposed with (i) uniform horizontal velocity equal to 0.12 m/s and vertical velocity equal to zero, (ii) uniform turbulent kinetic energy and dissipation rate equal to 0.00042 m^2/s^2 and 5.65×10^{-6} m^2/s^3, respectively, and (iii) uniform total SS concentration equal to

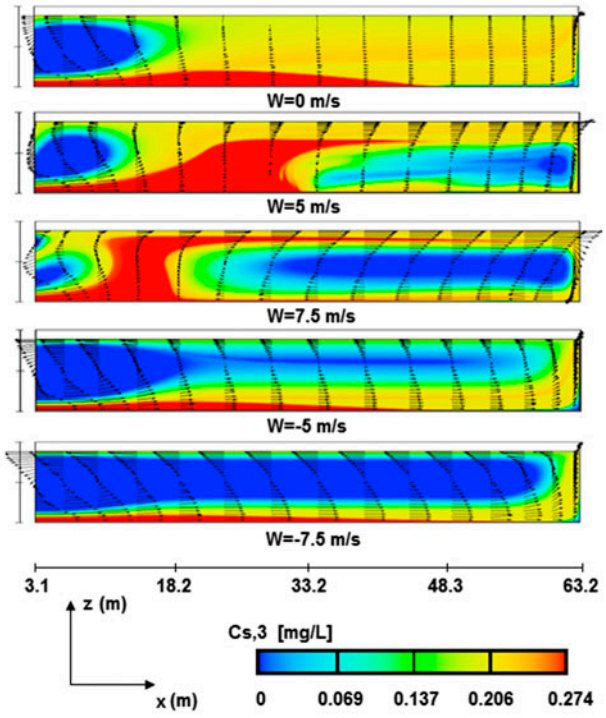

Fig. 2. Calculated flow velocity vectors and SS concentrations for class C3 and mode *A*.

7.0 mg/L. At the outlet of the tank, the pressure and the water height were specified. The bottom of the tank was treated as a no slip wall, while at the side walls the symmetry condition was applied. The location of free surface was defined using the VOF method [19]. The computational grid, which was finer at the inlet, the outlet and the bottom of the tank as well as near the water surface, consisted of approximately 51,300 cells with dimensions varying from 0.02 to 0.13 m; this grid was selected after a series of preliminary calculations to ensure grid independent results.

4.2. Scenarios of calculations

In order to investigate the effect of wind, we performed calculations for 10 scenarios; the first 5 scenarios for mode *A* of operation and the rest for mode *B*. The wind velocities were equal to 5.0, 7.5, −5.0, and −7.5 m/s; positive values indicate co-current wind direction and negative values indicate counter-current wind direction. In all scenarios, the movement of scraper was not modeled, but its effect was taken into account indirectly via the different percentages of the four classes of solids; i.e. for mode A we used the percentages of classes that were determined experimentally (see Table 1), while for mode *B* we employed the values that were determined after calibration and verification of the 3-D model that took into account indirectly the processes of resuspension and flocculation due to the presence of the sludge layer [9].

5. Results and discussion

Prior to the application of the model and due to the lack of hydrodynamic field data for the WTPA, the hydrodynamic part of the model was validated for the case of the primary sedimentation tank of the waste WTP in Sarnia, Ontario, Canada; this case has already been used in the past by various researchers for model validation (see, for example [21]). Calculated flow field of the present 2-D model showed a satisfactory agreement with field data, see Nitsa [23] for more details.

Figs 2 and 3 show flow velocity vectors and SS concentrations of Class C3 for mode A, and velocity profiles at various locations along the tank for $W = 7.5$ m/s, $W = 0$, and $W = -7.5$ m/s, respectively. In Fig. 4, calculated local removal efficiencies at the surface layer of the tank are compared with measurements for no-wind conditions, and in Table 2 the calculated removal efficiencies for all scenarios are shown.

Fig. 2 shows that for no-wind conditions, the flow is characterized by a relatively large recirculation region, above the inlet jet, which extends from $x = 0.0$ to $x \approx 20.0$ m and forces the flow to exit the tank following a short-circuiting route; this type of flow is typical for settling tanks with low concentrations of SS and, thus, no density effects [21]. The calculated length of the recirculation area (20.4 m) is approximately the same with the experimental value (20.0 m); see Section 3.2. Moreover, the length of the created sludge layer is approximately equal to 45.8 m; this value is practically the same with the experimental value (45.0 m); see Section 3.2.

For windy conditions, a two-layer flow is developed, in which the surface layer follows the wind direction; this two-layer flow was also observed in the 3-D calculations of Stamou and Gkesouli [9] that were performed for a strong co-current wind of 15 m/s. With increasing co-current wind, the upstream bottom layer suppresses the incoming jet and directs it towards the surface and finally towards the outlet, thus increasing the degree of short-circuiting. For counter-current wind, the surface layer flows upstream and the incoming jet forms the bottom layer that flows downstream and reaches the outlet at relatively high times, i.e. short-circuiting decreases; this

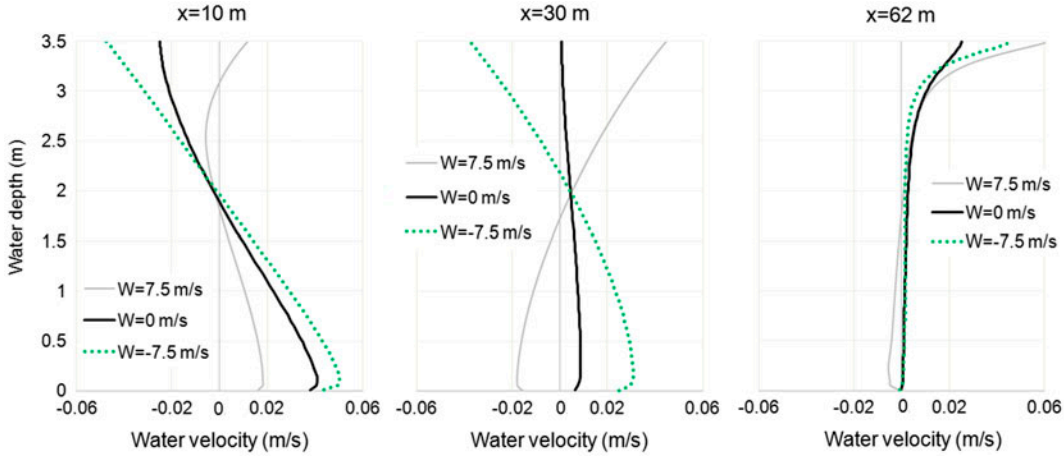

Fig. 3. Velocity profiles at various locations along the tank for mode *A*.

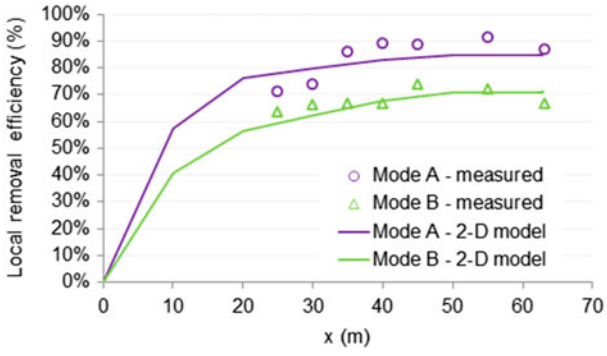

Fig. 4. Calculated and measured local removal efficiency at the surface of the tank for no-wind conditions for modes *A* and *B*.

Table 2
Calculated SS removal efficiencies for all scenarios

Wind velocity (m/s)	Mode *A* (%)	Mode *B* (%)
0.0	83.1	68.1
5.0	82.9	67.7
7.5	82.8	67.4
−5.0	83.7	68.8
−7.5	84.0	69.4

decrease is more pronounced for high values of wind velocity. Fig. 3 depicts that far from the inlet and outlet regions, the velocity distributions for opposite wind directions of the same magnitude (i.e. 7.5 and −7.5 m/s) are virtually symmetrical. The SS iso-concentration contours of Fig. 2 show that the concentration field depends strongly on the flow field, for example, in regions with intense mixing (i.e. in the recirculation area for no-wind conditions and near the interface of the two layers for windy conditions), the concentration profiles are more uniform. As expected, with increasing co-current wind velocity the iso-concentration contours are shifted upwards, towards the water surface, after being influenced by the upstream bottom current; thus, the outlet concentration increases and the efficiency of the tank is reduced. For counter-current wind velocities, the incoming flux of solids is carried away by the bottom current, i.e. along the bottom of the tank; subsequently, the outlet concentration decreases and the efficiency of the tank increases.

The aforementioned effects of the flow and concentration fields on the removal efficiency of the tank are shown in Fig. 4 and in Tables 2 and 3. Fig. 4 depicts that the calculated local removal efficiencies for no-wind conditions at the surface layer of the tank, downstream of the recirculation region ($x > 20$ m), are in satisfactory agreement with their corresponding values based on measurements. Table 2 shows that for no-wind conditions the removal efficiency is calculated equal to 83.1%; this value is in satisfactory agreement, however lower than the experimental value (86.0 ± 1.0%) and the value determined by a 3-D model (85.7%); with increasing co-current wind velocity (up to 7.5 m/s) the efficiency of the tank decreases, however not noticeably (<0.3%), while for increasing counter-current wind velocity the removal efficiency increases by up to approximately 1%; this behavior is in agreement with field observations (see Section 3.2). In Table 4, the calculated removal efficiency for each class, for all wind velocities and directions, is shown; as expected (see Section 3.2) the removal efficiencies of the heavy particles (class C1) are

Table 3
Calculated SS removal efficiencies for all classes for Mode *A* without wind

Class (–)	$u_{set,i}$ (m/h)	p_{in} (%)	C_{in} (mg/L)	Hazen number (–)	R_{ideal} (%)	R (%)
C1	5.80	70.0	4.9	6.80	100.0	99.6
C2	0.96	20.5	1.4	1.12	100.0	58.1
C3	0.31	4.0	0.3	0.36	36.0	25.4
C4	0.09	5.5	0.4	0.11	11.0	9.0
Sum	–	100	7.0	–	92.5	83.1

Table 4
Calculated SS removal efficiencies for all classes for Mode *A* for all wind velocities and directions

Class (–)	$u_{set,i}$ (m/h)	Hazen number (–)	R (%) $W = -7.5$ m/s	R (%) $W = -5.0$ m/s	R (%) $W = 5.0$ m/s	R (%) $W = 7.5$ m/s
C1	5.80	6.80	100.0	100.0	99.6	99.6
C2	0.96	1.12	59.7	58.7	57.6	57.3
C3	0.31	0.36	27.8	27.3	23.7	22.5
C4	0.09	0.11	11.0	10.9	7.7	6.9
Sum	–	–	84.0	83.7	82.9	82.8

practically equal to 100% and independent of the wind velocity and direction, while efficiencies for the lighter particles (classes C2, C3 and C4) are affected by wind characteristics.

When the sludge removal mechanism is not in operation (mode *B*), the flow field remains unaffected since the mechanism is not modeled and the concentrations of the SS remain very low (<7.0 mg/L) without creating density currents that may affect the flow field. However, the SS concentration field and the efficiency of the tanks change. Fig. 4 and Table 2 show that for mode *B* and no-wind conditions the calculated efficiency decreases from 83.1 to 68.1% (i.e. by 15%); this value is again lower than the experimental range of values (70.8 ± 1%) and the predicted by a 3-D model (70.9%) [9]. The effect of the wind shows a similar behavior as for mode *A*; however, this effect is more pronounced showing a difference of up to 1.3%.

6. Conclusions

The application of a 2-D CFD model in the settling tanks of the WTPA showed that the effect of sludge scraper on the removal efficiency of the tank is very important. For no-wind conditions and when the scraper is operating the efficiency is calculated equal to 83.1%, a value that is lower than the experimental value (86.0 ± 1.0%) and the prediction with a 3-D model (85.7%). Similarly, when the scraper is not in operation the removal efficiency is equal to 68.1%, a value that is again lower than the experimental value (70.8 ± 1.0%) and the predicted value by a 3-D model (70.9%). In other words, calculations with a 2-D model are satisfactory; however, they are less accurate than these with a 3-D model. The effect of co-current or counter-current wind velocity of up to 7.5 m/s on the flow and suspended concentration fields is important. However, this effect is not significant on the removal efficiency, which is approximately equal to 1% when the sludge scraper is in operation and 1.3% when the scraper is out of operation.

Acknowledgments

The present work was conducted within the framework of a research project entitled "Improving the settling efficiency in the old unit of WTP of Aharnes using modern flocculants and appropriate mathematical models, for parametrization in real operation conditions." The financial support by EYDAP Athens Water Supply and Sewerage Company S.A. for this project is gratefully acknowledged. Furthermore, the authors would like to thank the members of the Project Monitoring Committee: Mr A. Magoulas, Mrs M. Xanthaki, Mrs A. Synodinou, Dr F. Miskaki, Dr N. Defteraios, Dr T. Kaloudis, Dr E. Smeti and other scientific and technical personnel of EYDAP S.A., for the useful discussions and for providing the required information and data. A part of this work was carried out within the MSc Thesis of the second author in the TUM under the supervision of the third author, while he was Visiting Professor at the TUM; thanks are also due to the DAAD, the TUM, and the NTUA.

List of symbols

A^i — fractional area open to the flow in the i direction
c_D — drag coefficient
$c_{s,i}$ — volume concentration of class i
$C_{s,i}$ — mass concentration of class i
C_{in} — concentration of SS at the inlet of the tank
$d_{c,i}$ — characteristic diameter of class i
$d_{r,i}$ — range of diameter of class i
D — diffusivity
DDif — diffusion (ε transport equation)
Diff — diffusion (k transport equation)
f^i — viscous acceleration in the i direction
F — volume fraction
G — buoyancy production
G^i — body acceleration in the i direction
k — turbulence kinetic energy
p_{in} — percentage of classes at the inlet of the tank
P — pressure
P_s — shear production
t — time
$\overline{u^i}$ — bulk velocity of water–SS mixture in the i direction
$u_{s,i}$ — velocity of class i
$u_{set,i}$ — settling velocity of class i
u_w — water velocity
V_F — fractional volume open to the flow
W — wind velocity at height 10 m above water surface
x^i — Cartesian coordinate in the i-direction
ε — turbulence dissipation rate
μ — dynamic viscosity
μ_{tot} — total dynamic viscosity
μ_T — eddy viscosity
$\overline{\rho}$ — bulk density of the water–SS mixture
ρ_a — air density
ρ_s — density of SS
ρ_w — density of water
τ — shear stress on water surface
τ^i_{bx} — wall shear stress
$\tau_{x^i x^j}$ — strain rate tensor

References

[1] M. Shahrokhi, F. Rostami, M.Md. Said, S. Syafalni, Numerical investigation of baffle effect on the flow in a rectangular primary sedimentation tank, World Acad. Sci. Eng. Technol. 58 (2011) 332–337.
[2] A. Tamayol, B. Firoozabadi, G. Ahmadi, Effects of inlet position and baffle configuration on hydraulic performance of primary settling tanks, J. Hydraul. Eng. 134(7) (2008) 1004–1009.
[3] A.M. Goula, M. Kostoglou, T.D. Karapantsios, A.I. Zouboulis, A CFD methodology for the design of sedimentation tanks in potable water treatment: Case study: The influence of a feed flow control baffle, Chem. Eng. J. 140(1–3) (2008) 110–121.
[4] A.I. Stamou, G. Theodoridis, K. Xanthopoulos, Design of secondary settling tanks using a CFD model, J. Environ. Eng. 135(7) (2009) 551–561.
[5] H. Asgharzadeh, B. Firoozabadi, H. Afshin, Experimental and numerical simulation of the effect of particles on flow structures in secondary sedimentation tanks, J. Appl. Fluid Mech. 5(2) (2012) 15–23.
[6] G.A. Ekama, P. Marais, Assessing the applicability of the 1D flux theory to full-scale secondary settling tank design with a 2D hydrodynamic model, Water Res. 38 (2004) 495–506.
[7] M. Sivakumar, S.A. Lowe, Simulation of the effect of wind on rectangular sedimentation tanks, Conference on Hydraulics in Civil Engineering, Sydney, 1990, pp. 74–78.
[8] S.M. Khezri, A. Biati, Z. Erfani, Determination of the effect of wind velocity and direction changes on turbidity removal in rectangular sedimentation tanks, Water Sci. Technol. 66(12) (2012) 2814–2820.
[9] A. Stamou, A. Gkesouli, Modeling settling tanks for water treatment using computational fluid dynamics, J. Hydroinf. 17(5) (2015) 745–762.
[10] N.T.U.A, Improving the settling efficiency in the old unit of WTP of Aharnes using modern flocculants and appropriate mathematical models, for parametrization in real operation conditions, Research project, Final Technical Report, Athens, 2015.
[11] D.T. Tsahalis, Theoretical and experimental study of wind- and wave-induced drift, J. Phys. Oceanogr. 9(6) (1979) 1243–1257.
[12] Flow Science Inc., *FLOW—3D User's Manual*, Flow Science Inc, 2014.
[13] M. Shahrokhi, F. Rostami, M. Md Said, S. Syafalni, Numerical modeling of the effect of the baffle location on the flow field, sediment concentration and efficiency of the rectangular primary sedimentation tanks, World Appl. Sci. J. 15(9) (2011) 1296–1309.
[14] G. Wei, J. Brethour, M. Grünzner, J. Burnham, Sedimentation scour model, Flow Sci. Report 03–14, 2014.
[15] J.-M. Hervouet, Hydrodynamics of Free Surface Flows, John Wiley and Sons Ltd, Chichester, 2007.
[16] W. Rodi, Turbulence Models and Their Application in Hydraulics, third ed., IAHR, Rotterdam, 2008.
[17] V. Yakhot, S.A. Orszag, Renormalization group analysis of turbulence. I: Basic theory. J. Sci. Comput. 1 (1986) 1–51.
[18] V. Yakhot, L.M. Smith, The renormalization group, the e-expansion and derivation of turbulence models, J. Sci. Comput. 7 (1992) 35–61.
[19] C.W. Hirt, B.D. Nichols, Volume of fluid (VOF) method for the dynamics of free boundaries, J. Comput. Phys. 39 (1981) 201–225.
[20] I. Celik, W. Rodi, A.I. Stamou, Prediction of hydrodynamic characteristics of rectangular settling tanks, in: C.J. Chen, L.-D. Chen, F.M. Holly Jr., Turbulence Measurements and Flow Modelling, Part II: Computational Fluid Dynamics, Hemisphere Publishing Corp., New York, NY, 1987, pp. 641–651.
[21] A.I. Stamou, E.W. Adams, W. Rodi, Numerical modeling of flow and settling in primary rectangular clarifiers, J. Hydraul. Res. 27(5) (1989) 665–682.

[22] American Public Health Association, American Water Works Association and Water Environment Federation, Standard methods for the examination of water and wastewater, twenty-first ed., Washington, DC, 2005.

[23] M. Nitsa, Examining the effect of wind on the hydrodynamic behavior and efficiency of settling tanks using a CFD model, (MSc Thesis), TUM, Department of Hydraulic and Water Resources Engineering, 2015.